

PPD: A New Valet Parking Pedestrian Fisheye Dataset for Autonomous Driving

Zizhang Wu, Xinyuan Chen, Fan Song, Yuanzhu Gan, Tianhao Xu, Jian Pu*, Rui Tang*

Abstract—Pedestrian detection under valet parking scenarios is fundamental for autonomous driving. However, the presence of pedestrians can be manifested in a variety of ways and postures under imperfect ambient conditions, which can adversely affect detection performance. Furthermore, models trained on public datasets that include pedestrians generally provide suboptimal outcomes for these valet parking scenarios. In this paper, we present the Parking Pedestrian Dataset (PPD), a large-scale fisheye dataset to support research dealing with real-world pedestrians, especially with occlusions and diverse postures. PPD consists of several distinctive types of pedestrians captured with fisheye cameras. Additionally, we present a pedestrian detection baseline on PPD dataset, and introduce two data augmentation techniques to improve the baseline by enhancing the diversity of the original dataset. Extensive experiments validate the effectiveness of our novel data augmentation approaches over baselines and the dataset’s exceptional generalizability.

Index Terms—Datasets, Pedestrian detection, Data augmentation, Valet parking

I. INTRODUCTION

To develop an advanced driver assistance system (ADAS) that is both effective and safe for parking lot scenarios [1]–[5], it is critical to ensure the safety of road users such as pedestrians. The detection range of conventional pinhole cameras is often insufficient to detect the variety of behaviors and postures displayed by pedestrians. As an alternative to pinhole cameras, fisheye cameras could have a wider field of vision (FoV) [6], which is necessary for the perception of close range and low altitude, particularly in a traffic bottleneck. Thus, fisheye cameras are becoming increasingly prominent in driverless vehicles as intelligent alternatives to traditional cameras.

Nevertheless, such pedestrian detection [7]–[10] still remains difficult due to evasive irregular postures and imprecise surrounding circumstances. First, there is a wide range of pedestrian behaviors that are rarely represented in publicly available datasets, such as occlusion, lying down, walking, etc.

This paper was produced by Fudan University and Zongmu Technology. Zizhang Wu, Xinyuan Chen and Fan Song contributed equally to this work. Corresponding author: Jian Pu, Rui Tang.

Zizhang Wu, Jian Pu (e-mail: wuzizhang87@gmail.com; jianpu@fudan.edu.cn) is with Fudan University, No. 220, Handan Road, Shanghai, China.

Xinyuan Chen, Fan Song, Yuanzhu Gan, Tianhao Xu and Rui Tang are with the Zongmu Technology (Shanghai) Co., Ltd, Building 10, Zhangjiang Artificial Intelligence Island, Lane 55, Chuanhe Road, Pudong New Area, Shanghai, China. (e-mails: lan.chen@zongmotech.com; fan.song@zongmotech.com; yuanzhu.gan@zongmotech.com; tobias.xu@zongmotech.com; rui.tang@zongmotech.com)

Manuscript received xx xx, 2023; revised xx xx, 2023.

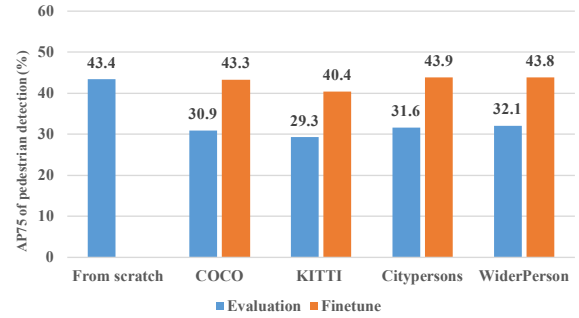


Fig. 1. The cross-dataset testing on the **PPD** dataset. “Evaluation” refers to explicitly evaluating public datasets’ pre-trained models on the **PPD** dataset, with suboptimal results compared with the model trained from scratch. “Finetune” means finetuning these pre-trained models on the **PPD** dataset with little advancement.

Second, the fisheye lens’s radial distortion leads to substantial appearance distortion [11], [12], complicating the pedestrian recognition process. Additionally, the quality of images is significantly affected by environmental factors such as light and opacity.

Current datasets and benchmarks for pedestrian detection, including Caltech USA [13], KITTI [14], CityPersons [15], and Wider-Person [16], have aided in rapid progress for the pedestrian detection task. These datasets usually encompass urban, rural, or highway driving scenes, and their pinhole cameras comfortably capture high-grade images with clear and distinguishable pedestrians. Moreover, Valeo delivers the fisheye automotive dataset WoodScape with extensive content [17]. However, public datasets place insufficient emphasis on pedestrians with irregular postures and fisheye image formation. The models trained on public datasets reveal suboptimal performance in difficult parking scenes without a large number of training instances, as shown in Fig.1 and Fig.2.

To expand real-world fisheye pedestrians’ images with various occlusion and postures under valet parking scenes, this paper offers a new large-scale fisheye dataset called **Parking Pedestrian Dataset (PPD)** to promote the research on pedestrian problems, as shown in Figure 2 (b). Different from other pedestrian datasets [13]–[16], our **PPD** dataset focuses on pedestrian detection and provides more than 330K fisheye images in valet parking scenes. To guarantee the pedestrians’ diversity, we collect data from different parking lots, various periods, and diverse pedestrian situations. Additionally, we subdivide **PPD** into three sub-datasets: Occlusion Pedestrians (**OP**), Posture Pedestrians (**PP**), and Lying-down Pedestrians (**LP**). **OP** involves pedestrians occluded by car bodies, doors,



Fig. 2. Green boxes indicate ground truth and red boxes indicate predictions. (a) The suboptimal performance of the detector pre-trained on public datasets in parking lot scenes. (b) Our **Parking Pedestrian Dataset (PPD)** uses data augmentation methods and provides diverse large real-world pedestrian data with occlusion and different postures.

or parking lots’ pillars. **PP** is concerned with pedestrians’ abundant postures, including standing, stooping, sitting, etc. **LP** concentrates on lying-down pedestrians, the most perilous situation that requires immediate early warning.

To reduce annotation costs and further broaden the diversity of pedestrians, we further propose two data augmentation techniques: **Occ-Data-Augmentation (ODA)** and **Pos-Data-Augmentation (PDA)** for pedestrians’ occlusions and postures, respectively. Using **ODA** and **PDA**, high-quality synthetic images are generated through the collecting, localization, and local fusion procedures, complementing the commonly used hybrid augmentation methods [18]–[20]. Besides, we build pedestrian detection baselines on our **PPD** dataset and extensive experiments validate the effectiveness of our novel data augmentation approaches. In addition, the cross-dataset evaluation reveals **PPD**’s exceptional capacity to generalize.

Our contributions are summarized as follows:

- We provide the first fisheye dataset comprising over 330K fisheye images, particularly for diverse occlusion and postures of pedestrians in parking lot scenes.
- We report the baseline results of pedestrian detection on the proposed **PPD** dataset and propose two novel data augmentation techniques to improve the baseline.
- Extensive experiments demonstrate the effectiveness of **ODA**, **PDA**, and **PPD**’s exceptional generalizability.

II. RELATED WORK

In this section, we briefly introduce the related works to our topic, i.e., pedestrian detection dataset, pedestrian detection frameworks, and data augmentation methods.

A. Pedestrian Detection Datasets

Pioneer works of pedestrian detection datasets involve [13]–[16], [21]–[25], which contribute to great progress in pedestrian detection. There are large-scale datasets such as Caltech

USA [13] and KITTI [14], which contain urban, rural, and highway scenes and provide annotation frame sequences on videos. However, both datasets have low pedestrian densities. More recently, researchers proposed vast and diversified datasets, WiderPerson [16] and CityPersons [15]. CityPersons [15] is the subset of the CityScapes Dataset, whose average pedestrian density grows three times that of KITTI [14]. WiderPerson [16] contains a range of scenarios, including marathon, traffic, activity, dance, and miscellany, totaling approximately 400 thousand annotated instances. Moreover, Valeo proposed the extensive automotive dataset WoodScene [17] with fisheye cameras instead of pinhole cameras. However, there is no publicly available benchmark dataset for valet parking pedestrian scenarios, particularly those including varied occlusions and postures, where suboptimal detection of pedestrians forms a threat to driving safety.

B. Pedestrian Detection Frameworks

CNN-based pedestrian detection methods can be generally categorized into one-stage [26]–[28] and two-stage [29], [30] methods. As an end-to-end pipeline, one-stage methods achieve a significant trade-off between performance and speed, such as the SSD series [31]–[34], YOLO series [27], [28], [35], [36] and Retinanet [26]. In contrast, two-stage methods, such as the RCNN series [29], [30], [37], [38], take advantage of the predefined anchors to improve the performance at the cost of speed. Furthermore, recent works [39]–[42] fuse multi-scale feature maps to improve pedestrian detection with different scales. Moreover, other works [8], [9], [43]–[45] focus on crowded pedestrian detection problems for actual applications. [43] designed a new boundary box regression loss specifically for better pedestrian localization. Liu et al. offer a non-maximum suppression method to refine the bounding boxes given by detectors [44].

TABLE I
STATISTICS OF OUR COLLECTED PARKING PEDESTRIAN DATASET, WHICH CONSISTS OF THREE SUBDATASETS: OCCLUSION PEDESTRIAN DATASET, POSTURE PEDESTRIAN DATASET AND LYING-DOWN PEDESTRIAN DATASET. “#” DENOTES THE NUMBER.

Dataset	Sub-dataset	Image resolution	#images			#pedestrians		
			train	val	test	train	val	test
Parking Pedestrians	Occlusion Pedestrians (OP)	1280×580	51921	31900	27700	208659	105303	104211
	Posture Pedestrians (PP)	1920×870	52123	39080	27021	206401	140800	123120
	Lying-down Pedestrians (LP)	1920×870	53993	39022	22921	205300	103978	90090

C. Data Augmentation Methods

Data Augmentation methods such as random cropping, color dithering and flipping, play an important role in achieving state-of-the-arts [46]–[48]. These enhancements are more generic in nature and are particularly relevant to expressing data transformation invariance. In addition, hybrid image augmentation [18]–[20] can mix cross-image information, which usually applies appropriate changes with labels to increase diversity. Furthermore, the adaptations of mixups [20], [49], [50] are popular among hybrid image augmentation. CutMix [49] pastes a rectangular crop of the image instead of mixing all pixels. It creates new composite pictures by combining the rectangular grids of individual images with actual boxes. Cut-Paste-and-Learn [50] extracts objects in poses and then mixes and pastes them to different backgrounds. Copy-paste [20] fuses information from different images in an object-aware manner: copying and pasting instances across images.

III. PARKING PEDESTRIANS DATASET

In this section, we introduce our **Parking Pedestrian Dataset (PPD)** dataset in detail, including the data collection, annotation protocols, informative statistics, and dataset characteristics.

A. Data Collection

To ensure the diversity of pedestrians, we collect data from 3 cities, 12 parking lots, two periods (morning and evening), and different pedestrians with various ages, heights, clothes, and postures. In total, we captured 100 videos that last from 1 hour to 6 hours and with an average of 2 hours. Then, we convert the videos into pictures and select the images containing pedestrian instances. For high-quality images, we restrict the visible range of the fisheye camera and further remove distorted and blurred pedestrian images. Also, we do not cover all pedestrians’ continuous moving processes for redundant annotations. Instead, we select the best-quality images and then apply our data augmentation methods (discussed later) to increase the data variance. Based on the images’ content, we also divide them into three categories: occlusion pedestrians, posture pedestrians, and lying-down pedestrians.

Table I illustrates the statistics of the **PPD** dataset. A total of more than 330K images comprise three sub-datasets: Occlusion Pedestrians Dataset, Posture Pedestrians Dataset and Lying-down Pedestrians Dataset, with amounts of 111,521, 118,224 and 115,936, respectively. Besides, every sub-dataset further performs partitioning into training, validation and testing sets at a ratio of 5:3:2.

B. Image Annotation

We annotate the dataset in the same way as the Caltech dataset [22], by drawing a tight bounding box around each pedestrian’s complete body. However, occluded pedestrians are special since the foreground-like car bodies or parking lot pillars often lead to incomplete pedestrian instances. Therefore, we have to estimate the distance from the pedestrian instance to the car’s fisheye camera, and then roughly calculate the size of the box according to the depth proportion, as shown below:

$$W_o = W_p \times (1 - D_o/D_{max}), \quad (1)$$

$$H_o = H_p \times (1 - D_o/D_{max}), \quad (2)$$

where H_p and W_p are the average human height and width, predefined as 1.7 meters and 0.3 meters, respectively. D_o is the depth from the occluded pedestrian instance to the camera. Since the parking space has a fixed size, we can estimate the depth approximately by the relative location between the pedestrian instance and the nearby parking space within the same image. D_{max} is the max depth of the fisheye camera. Finally, based on the depth ratio between D_o and D_{max} , we can roughly infer the annotated width W_o and height H_o , as shown in Equations. (1) and (2).

C. Sub-datasets Description

The occluded pedestrian dataset provides three occlusion scenarios with different occlusion rates. As shown in Fig. 3, to better restore reality, we collect the pedestrians occluded by the cars’ part and cube obstacles with 10 occlusion rates, starting from not occluded to 99% with 10% increments per class.

The posture pedestrian dataset contains four postures: standing, sitting, squatting and bending over. We strive to cover eight pedestrians’ orientations, which are front, rear, left, right, left front, right front, left rear, and right rear. In addition, we divide lying-down pedestrians into the new subset since they are the most dangerous cases. We make an effort to cover the same eight orientations as the posture subset. The detailed distribution of posture and lying-down pedestrians is shown in Fig. 4, and a detailed explanation of **PPD**’s categories is reported in Table II.

Furthermore, to further broaden pedestrians’ diversity, we apply two novel data augmentation techniques to occlusion and posture pedestrians. The data volume increases, and later experiments will indicate improvements in pedestrian detection performance.



Fig. 3. Examples of different occlusion scales and occlusion types in the Occlusion Pedestrian Dataset.

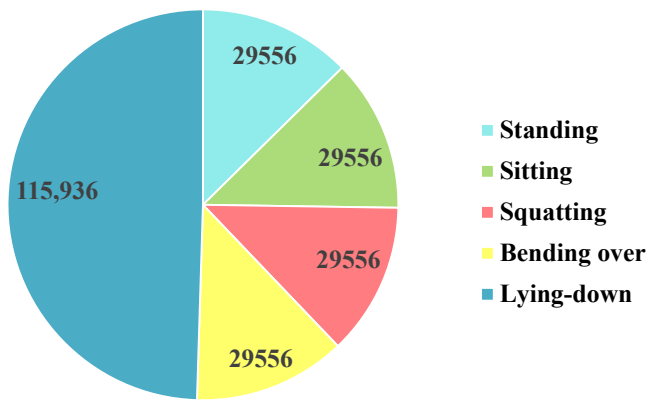


Fig. 4. The detailed distribution of posture pedestrian dataset and lying-down pedestrians dataset.

TABLE II
THE EXPLANATIONS FOR PPD’S CATEGORIES.

Category	Explanation	
Occlusion	Car’s front part	Pedestrians occluded by car’s front part
	Car’s rear part	Pedestrians occluded by car’s rear part
	Cube obstacle	Pedestrians occluded by cube obstacles like pillar or fire hose
Posture	Standing	Pedestrians with standing posture
	Sitting	Pedestrians with sitting posture
	Squatting	Pedestrians with squatting posture
	Bending over	Pedestrians with bending over posture
Lying-down	Lying-down pedestrians, independent of posture pedestrians	

D. Dataset Characteristics

Our PPD dataset exhibits differences from public datasets in image representation style, scenarios, quantity and diversity. Below, we elaborate on the four main characteristics of our PPD dataset.

Fisheye image representation. The PPD dataset consists of fisheye images, different from the common pinhole images of public datasets. Fisheye images provide a larger field-of-view (FoV), which is more suitable for close-range and low-lying pedestrian detection.

Specific parking scenarios. The PPD dataset focuses on pedestrian detection in parking scenarios, which is

also distinct from natural scenes of public datasets. The environmental conditions in parking scenarios, such as light and opacity, significantly increase the detection difficulty. Concerning a variety of tough pedestrian scenarios, PPD can promote research in dealing with real-world pedestrian problems.

Large quantity. Our PPD dataset obtains more than 330 thousand data samples from more than 200-hour parking scene video clips. We constantly collect diverse parking pedestrian scenarios, eventually reaching the goal of over one million data.

High quality and diversity. Our PPD dataset covers 3 cities, 12 parking lots from different periods and different pedestrian cases. Additionally, we carefully select high-quality images with high resolution and apply data augmentation techniques to enlarge diversity.

IV. THE PROPOSED DATA AUGMENTATIONS

Training detectors for special pedestrians usually requires a large quantity of data, which demands tremendous resources and effort to acquire and annotate. Considering these challenges, we provide two novel data augmentation techniques: **Occ-Data-Augmentation (ODA)** and **Pos-Data-Augmentation (PDA)**. Specifically, ODA focuses on occluded pedestrians, and PDA targets pedestrians with different postures. In this section, we describe those two data augmentation methods in detail.

A. Overall Pipeline

We define our data augmentation process as $f(*)$, so the overall structure states are as follows:

$$I_i^{syn} = f(I_i^{bg}, M_j), i = 1, 2, \dots, N, j = 1, 2, \dots, K \quad (3)$$

where I_i^{bg} is the background image, M_j indicates pedestrian masks and I_i^{syn} indicates the produced synthetic images.

As shown in Fig. 5, our augmentation pipeline contains three stages: (1) collecting pedestrian masks and background images; (2) determining where to paste pedestrian masks; and (3) fusing pedestrian masks with background images.

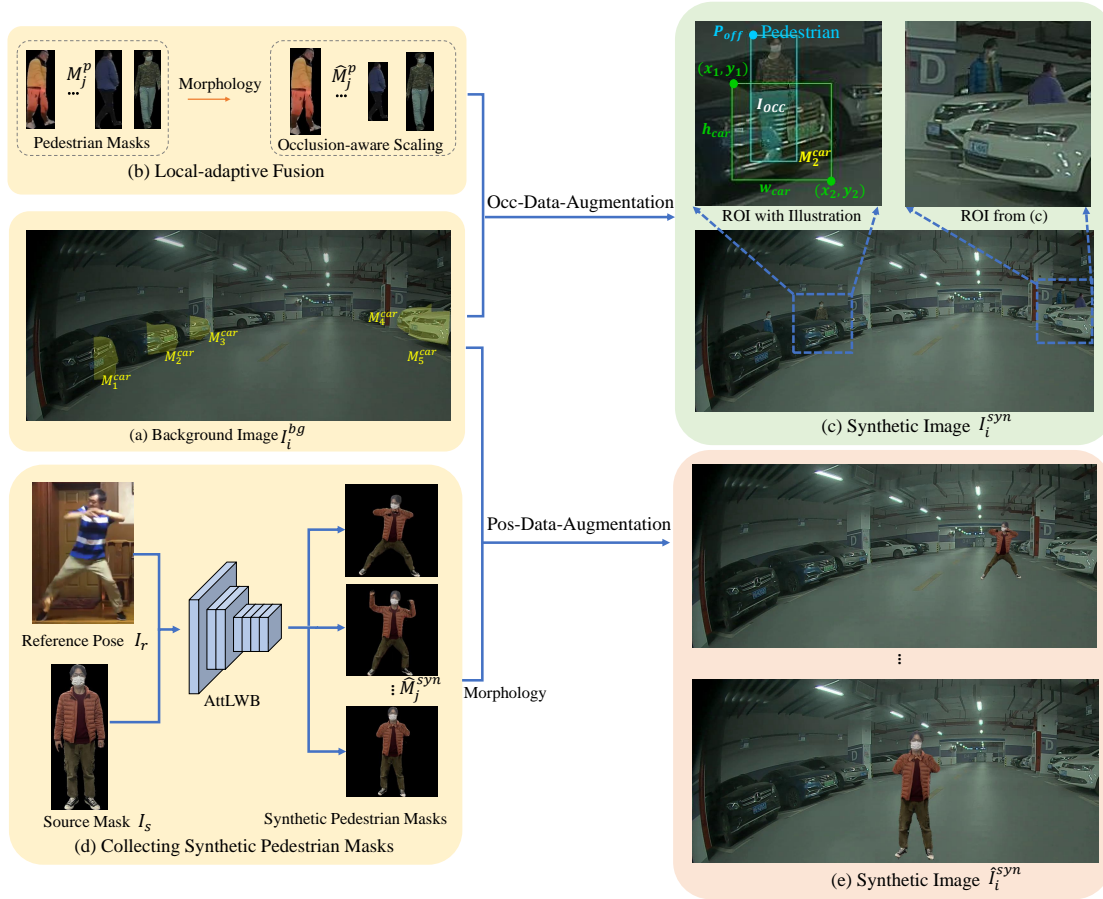


Fig. 5. Overview of our data augmentation methods. Our methods include **Occ-Data-Augmentation (ODA)** and **Pos-Data-Augmentation (PDA)**. **ODA** and **PDA** have the same pipeline: (1) collecting pedestrian masks and background images; (2) determining where to paste pedestrian masks; (3) fusing pedestrian masks with background images.

B. Occ-Data Augmentation

We present the **Occ-Data-Augmentation (ODA)** method for occluded pedestrians with three procedures. The detailed procedure can be found in Algorithm 1.

1) *Collecting pedestrian masks and background images:* We observe that in the valet parking scenes, cars' front or rear parts mostly occlude pedestrians. To address such occlusion, our **ODA** requires the masks of pedestrians $M_j^p, j = 1, 2, \dots, K$ as foreground and the background images $I_i^{bg}, i = 1, 2, \dots, N$, containing the masks of cars' front parts $M_i^{car}, i = 1, 2, \dots, N$.

For a background image, we label all available cars' front parts with the Labelme tool [51], as shown in Fig. 5 (a). Note that the pedestrian masks should be diverse and high quality, which determines the reality of the synthesized images. Thus, we process them with morphological operations such as OPEN and ERODE. To seamlessly paste pedestrian masks into background images, we apply occlusion-aware scaling, resizing the mask to a more realistic scale.

2) *Localization of synthetic occlusion:* Following Algorithm 1, we take one background image I_i^{bg} as input and randomly pick one car's front part M_t^{car} as the pasting location. Then, we prepare the pedestrian mask M_j^p , randomly selected from the mask list M^p .

3) *Local fusion for occlusion:* For more precise localization, we paste the top-left point P_{off} of the pedestrian mask above the car's front part M_t^{car} with random but limited distances, as shown in Fig. 5(d). Specifically, we calculate P_{off} according to:

$$P_{off} = \begin{bmatrix} x \\ y \end{bmatrix} = \begin{bmatrix} randint(x_1, x_2 - w_p') \\ y_1 - randint(0.2 * h_{car}, 0.3 * h_{car}) \end{bmatrix} \quad (4)$$

where w_p' is the width of the resized pedestrian mask and $(x_1, y_1), (x_2, y_2)$ are the top-left and bottom-right points of the front car part's mask. h_{car} and w_{car} are the corresponding width and height of the front car part's mask, respectively. It is noteworthy that all coordinates are relative to the top-left vertex. Furthermore, we remove the intersection between the pedestrian mask and the background, that is, the occlusion region: $I_{occ} = \widehat{M}_j^p \cap \widehat{M}_t^{car}$ (line 13 of Algorithm 1). In this way, we accomplish the pseudo occluded pedestrian's mask I_{avil}^{fg} . Then, we paste the pedestrian's mask into the background image and update the label, according to

$$I_i^{syn} = \alpha * I_{avil}^{fg} + (1 - \alpha) * I_i^{bg} \quad (5)$$

where $\alpha = 1.0$ with foreground and $\alpha = 0.0$ with background. Finally, we generate synthetic image I_i^{syn} with the pseudo label, as shown in the top row of Fig. 6.

Algorithm 1 Occ-Data-Augmentation

Require: pedestrian masks $M_j^p, j = 1, 2, \dots, K$; background images $I_i^{bg}, i = 1, 2, \dots, N$; front car parts' masks $M_i^{car}, i = 1, 2, \dots, N$

Ensure: $I_i^{syn}, i = 1, 2, \dots, N$

- 1: Fix random seed;
- 2: Shuffle I^{bg} and M^{car} ;
- 3: $i \leftarrow 1$;
- 4: **while** $i \leq N$ **do**
- 5: $\widehat{M}_t^{car}, t = 1, 2, \dots, T \leftarrow$ randomly select some of labels from M_i^{car} ;
- 6: **for** \widehat{M}_t^{car} in \widehat{M}^{car} **do**
- 7: $x_1, y_1, x_2, y_2 \leftarrow \widehat{M}_t^{car}$'s shape;
- 8: $w_{car}, h_{car} = x_2 - x_1, y_2 - y_1$;
- 9: $M_j^p \in \mathbb{R}^{w_p \times h_p} \leftarrow$ randomly select from M^p ;
- 10: Resize M_j^p to \widehat{M}_j^p with $w'_p = w_p \frac{h_{car}}{h_p}, h'_p = h_{car}$;
- 11: $P_{off} = (\text{randint}(x_1, x_2 - w'_p), y_1 - \text{randint}(0.2 * h_{car}, 0.3 * h_{car}))$;
- 12: $I_{occ} = \widehat{M}_j^p * \widehat{M}_t^{car}$ in P_{off} ;
- 13: $I_{avail}^{fg} = \widehat{M}_j^p - I_{occ}$;
- 14: $I_i^{syn} = \alpha * I_{avail}^{fg} + (1 - \alpha) * I_i^{bg}$;
- 15: Create pseudo label of I_{syn} ;
- 16: **end for**
- 17: $i \leftarrow i + 1$;
- 18: **end while**
- 19: **return** I^{syn} .

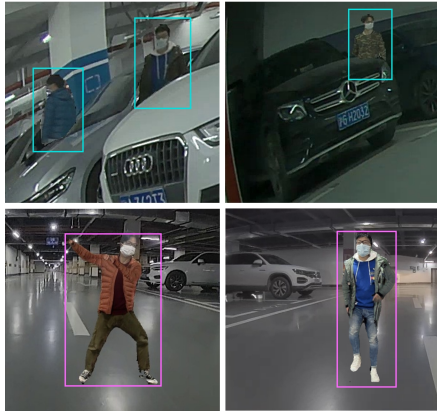


Fig. 6. Examples of augmented images. Top row: ODA results; Bottom row: PDA results.

C. Pos-Data-Augmentation

We illustrate our **Pos-Data-Augmentation (PDA)** method in Algorithm 2, which also contains three steps.

1) *Collecting pedestrian masks and background images:* Different from **ODA**, **PDA** only requires one source pedestrian image I_s and background images $I_i^{bg}, i = 1, 2, \dots, N$. The source image requires pedestrians with a complete body structure and black background, with the assistance of the Labelme tool [51]. Moreover, Liquid Warping GAN (AttLWB) [52] could create different human postures with a reference video, which warps the visible textures of source images to the desired poses. With the help of AttLWB [52], we obtain a series of synthetic pedestrian masks $M_j^p, j = 1, 2, \dots, K$

Algorithm 2 Pos-Data-Augmentation

Require: pedestrian masks $M_j^{syn}, j = 1, 2, \dots, K$, background images $\widehat{I}_i^{bg}, i = 1, 2, \dots, N$;

Ensure: $\widehat{I}_i^{syn}, i = 1, 2, \dots, N$.

- 1: Fix random seed;
- 2: Shuffle \widehat{I}^{bg} ;
- 3: $i \leftarrow 1$;
- 4: **while** $i \leq N$ **do**
- 5: $M_j^{syn} \leftarrow$ randomly select from M^{syn} ;
- 6: Randomly location P'_{off} from freespace of \widehat{I}_i^{bg} ;
- 7: $\widehat{I}_i^{syn} = \alpha * M_j^{syn} + (1 - \alpha) * \widehat{I}_i^{bg}$ in P'_{off} ;
- 8: Create pseudo label of \widehat{I}_i^{syn} ;
- 9: $i \leftarrow i + 1$;
- 10: **end while**
- 11: **return** \widehat{I}^{syn} .

with different pedestrian postures, as shown in Fig. 5(c). Furthermore, we also take the morphological operations OPEN and ERODE to process the synthetic pedestrian masks to remove the noise near the mask's contours.

2) *Localization of synthetic posture pedestrians.:* Since posture pedestrians must lie within the freespace region of parking scenes, we first detect the freespace region. We train a simple semantic segmentation model for freespace region detection and randomly pick one location within the model's freespace prediction. It is notable that this approach slightly requires time and computational resources, but we apply the procedure to ensure the quality of pseudo labels.

3) *Local fusion of pedestrian masks:* Finally, we resize the masks at a limited scale and paste the pedestrian masks into the background at the selected freespace location:

$$\widehat{I}_i^{syn} = \alpha * M_j^{syn} + (1 - \alpha) * \widehat{I}_i^{bg}. \quad (6)$$

Then, we obtain synthetic posture pedestrians with pseudo labels, as shown in Fig. 5 (e). The bottom row of Fig. 6 illustrates the **PDA**'s examples.

V. EXPERIMENTS

In this section, we report the baseline results and the results of two proposed data-augmentation techniques on our **PPD** dataset. Then, we discuss **PPD**'s generalization across datasets. Furthermore, we analyze the effects of **ODA** and **PDA** by ablation studies and comparisons.

A. Experimental Settings

1) *Implementation Details:* We conduct experiments with the Pytorch framework on Ubuntu system and employ eight NVIDIA RTX A6000s. The learning rate is set to 0.12, while the momentum and learning decay rates are set to 0.9 and 0.01, respectively. For training, we adopt the stochastic gradient descent (SGD) solver, 48 epochs, and 16 batch size. For our data augmentation experiments, we mix 250,000 augmentation images with the original **PPD** dataset.

TABLE III

THE PERFORMANCE OF BASELINES ON OUR **PPD** DATASET WITHOUT OR WITH DATA-AUGMENTATION IMAGES (PPD w/ DA).

Method	PPD		PPD w/ DA		Improvement	
	AP75	AR75	AP75	AR75	AP75	AR75
CenterNet	43.4	52.7	46.6	55.7	+3.2	+3.0
YOLOF	52.1	40.3	54.3	43.1	+2.2	+2.8
Faster RCNN	54.1	43.3	57.4	45.3	+3.3	+2.0
Cascade RCNN	54.0	42.7	56.9	45.1	+2.9	+2.4
RetinaNet	51.0	41.3	54.1	44.5	+3.1	+3.2

TABLE IV

THE PERFORMANCE OF CENTERNET ON SUB-DATASETS WITHOUT OR WITH DATA-AUGMENTATION IMAGES (w/ DA).

Subdataset	AP75	AR75
Occlusion Pedestrians	41.3	51.2
Occlusion Pedestrians w/ DA	44.3	54.4
Posture Pedestrians	43.5	53.9
Posture Pedestrians w/ DA	45.7	56.3

2) *Evaluation Metrics*: The detection task ought to chase superb targets for the location to ensure pedestrians’ safety. Therefore, we select a high IoU criterion of 0.75 for object detection metrics: Average Precision (AP) and Average Recall (AR). The high threshold forms a stricter examination to filter more robust models for the pedestrian detection task.

3) *Baseline methods*: Our baseline detectors contain CenterNet [53] with backbone DLA34 [54], YOLOF [35], Faster R-CNN [37], Cascade RCNN [55] and RetinaNet [26] with ResNet-50 [56] backbone. All baselines have occupied the field of object detection in recent years. To ensure comparability, all baselines utilize the same experimental settings as their release.

4) *Datasets*: We also choose several public datasets for cross-dataset evaluation: COCO [21], KITTI [14], CityPersons [15], and WiderPerson [16], where the last two datasets aim for the category “Person”.

B. Results and Analysis

1) *Results on PPD and PPD w/ DA*: To demonstrate the effectiveness of our data-augmentation methods, we conduct baseline evaluation based on the **PPD** dataset and the mixed dataset with augmentation images, as shown in Table III. For the original **PPD** dataset, the two-stage Faster RCNN wins on AP75, and the one-stage CenterNet wins on AR75. As a new anchor-free pipeline, CenterNet focuses on object center detection, which brings higher recall and perhaps lower precision. All the performance enhancements are approximately 2% to 4% when mixed with data-augmentation images. We attribute the advancement to our realistic synthetic images, which satisfy the appetite of pedestrians with various occlusions and postures at a low cost.

Besides, we explore the subdatasets’ performance with data-augmentation images (w/ DA), as shown in Table IV. Additional data-augmentation images take effect individually on both sub-datasets.

TABLE V

EVALUATION OF THE GENERALIZABILITY OF PUBLIC DATASETS TO THE **PPD** DATASET BASED ON THE CENTERNET [53] METHOD. A→B MEANS ADOPTING THE MODEL PRETRAINED ON DATASET A TO EVALUATE OR FINETUNE ON DATASET B.

Dataset	Evaluation		Finetune	
	AP75	AR75	AP75	AR75
PPD (from scratch)	43.4	52.7	-	-
COCO →PPD	30.9	34.7	43.3	52.5
KITTI →PPD	29.3	33.2	42.5	52.3
Citypersons →PPD	31.6	35.3	43.7	53.1
WiderPerson →PPD	32.1	36.9	43.6	53.0

TABLE VI

EVALUATION OF THE GENERALIZABILITY OF THE **PPD** DATASET TO PUBLIC DATASETS BASED ON CENTERNET [53]. A⇒B MEANS ADOPTING THE MODEL PRE-TRAINED ON DATASET A TO FINETUNE ON DATASET B.

Dataset	AP75	AR75
COCO	44.7	38.7
PPD⇒COCO	47.2	42.5
KITTI	52.3	56.2
PPD⇒KITTI	55.8	59.8
Citypersons	46.5	57.3
PPD⇒Citypersons	49.1	58.8
WiderPerson	53.3	47.9
PPD⇒WiderPerson	56.7	53.1

2) *Cross-dataset Evaluation*: First, we test how well models, which perform well on commonly used datasets, perform on our **PPD** dataset. We train CenterNet models on the public datasets COCO, KITTI, CityPersons, and WiderPerson. Then, we infer and evaluate them on the **PPD** dataset, as shown in Table V. We observe that models pre-trained on public datasets perform suboptimally, indicating their inadequacy with irregular pedestrian fisheye instances. Furthermore, we finetune these models on the **PPD** dataset, also as shown in Table V. In comparison to the **PPD** model trained from scratch, the pre-trained cross-dataset models do not make much advancement, even with a small performance drop similar to the KITTI dataset. We conjecture that public datasets are insufficient to compensate for the absence of different pedestrians with occlusion and varied postures.

Moreover, we conduct generalization experiments from **PPD** on public datasets based on CenterNet [53], as shown in Table VI. After finetuning, our **PPD** dataset gains approximately 2% to 5% enhancement compared to the baselines trained on public datasets, especially for AR 75. **PPD**’s pedestrian cases cover the usual pedestrian scenes, which considerably increases the recall and lift generalization ability.

3) *Ablation Study*: We conduct ablation studies for the **Occ-Data-Augmentation (ODA)** and **Pos-Data-Augmentation (PDA)** methods based on CenterNet [53], as shown in Table VII. (b) and (c) rows show that training only with synthetic images does not make sense because of the data domain shift. From rows (d) and (e), our **ODA** and **PDA** obviously make great progress, especially **ODA**, contributing approximately 2% AP75 improvement. Both techniques are effective, and the result performs best in combination, as shown in the (f)

TABLE VII

ABLATION STUDY OF TWO DATA-AUGMENTATION TECHNIQUES, ODA AND PDA, BASED ON THE CENTERNET METHOD.

	PPD	ODA	PDA	AP75	AR75
(a)	✓			43.4	52.7
(b)		✓		30.6	36.7
(c)			✓	28.4	33.2
(d)	✓	✓		45.6	54.3
(e)	✓		✓	44.5	53.4
(f)	✓	✓	✓	46.6	55.7

TABLE VIII

COMPARISON BETWEEN OUR DATA-AUGMENTATION METHOD AND THE COPY-PASTE METHOD WITH THE SAME CENTERNET METHOD, BASED ON THE PPD DATASET.

	Method	AP75	AR75
(a)	PPD	43.4	52.7
(b)	PPD w/ Copy-paste	37.2	48.1
(c)	PPD w/ DA	46.6	55.7

TABLE IX

EXPLORATION OF THE OPTIMAL QUANTITY FOR DATA-AUGMENTATION APPROACHES USING THE CENTERNET METHOD AND THE PPD DATASET. THE GREATEST AMOUNT OF TRAINING DATA MAY NOT ALWAYS PROVIDE THE BEST RESULTS.

	Amount	AP75	AR75
(a)	+ 0	43.4	52.7
(b)	+ 50,000	44.1	52.9
(c)	+ 150,000	45.3	53.4
(d)	+ 250,000	46.6	55.7
(e)	+ 350,000	46.1	54.2
(f)	+ 450,000	45.9	53.3

row.

4) **Comparison with Copy-paste:** Copy-paste [20] plays an important role in hybrid image augmentation. We compare our data-augmentation techniques with copy-paste based on CenterNet, as shown in Table VIII. Surprisingly, from (b) row, the model’s performance with copy-paste degrades by approximately 5%. We analyze copy-paste copies and paste instances across images but without any fusion processing, which easily leads to unreliable images and false detection. In contrast, our well-organized adaptive pasting localization and fusion strategies bring an improvement of 3.2% in AP75 and 3.0% in AR75 in the (c) row.

5) **Discussion with amount of data-augmentation images:** Theoretically, we could produce infinite pseudo-labeling images. However, a large quantity of training data occupies large amounts of resources and time. To trade off the efficiency and performance, we explore the optimal quantity for pseudo-labeling images based on the CenterNet [53] method and the PPD dataset, as shown in Table IX. Interestingly, from rows (d), (e) and (f), most training data do not perform the best result, perhaps resulting from overfitting. Before overfitting, a larger image volume means greater enhancement, as illustrated in rows (b), (c) and (d).

VI. CONCLUSION

In this paper, we have presented a new dataset, the Parking Pedestrians Dataset (**PPD**), as well as two unique data-augmentation techniques, Occ-Data-Augmentation (**ODA**) and Pos-Data-Augmentation (**PDA**). By providing a diversity of pedestrian postures, the proposed dataset aims to assist the industry in constructing a more secure advanced driving assistance system. Moreover, we provide two techniques for enhancing pedestrian detection performance using data augmentation. Extensive experiments on the proposed PPD validate the effectiveness of the techniques. However, PPD has a large capacity for development, including how to strengthen the realism of the data augmentation, simplify our methodologies, deal with sustainably increasing data and have the potential for diverse vision tasks. Nevertheless, we expect PPD to inspire more relevant research and promote the performance of pedestrian detection under parking scenes. In the future, the proposed PPD dataset’s potential not only lies in pedestrian detection but can also be extended into other vision tasks, such as pixel-wise semantic segmentation, video object detection and 3D object detection tasks.

REFERENCES

- [1] Z. Wu, M. Wang, J. Wang *et al.*, “Deepword: A gcn-based approach for owner-member relationship detection in autonomous driving,” in *IEEE International Conference on Multimedia and Expo(ICME)*, 2021, pp. 1–6.
- [2] Z. Wu, W. Sun, M. Wang *et al.*, “Psdet: Efficient and universal parking slot detection,” in *IEEE Intelligent Vehicles Symposium(IV)*, 2020, pp. 290–297.
- [3] B. Li, Z. Yin, Y. Ouyang *et al.*, “Online trajectory replanning for sudden environmental changes during automated parking: A parallel stitching method,” *IEEE Transactions on Intelligent Vehicles*, 2022.
- [4] J. Wu, Z. Huang, and C. Lv, “Uncertainty-aware model-based reinforcement learning: Methodology and application in autonomous driving,” *IEEE Transactions on Intelligent Vehicles*, 2022.
- [5] M. Biparva, D. Fernández-Llorca, R. I. Gonzalo *et al.*, “Video action recognition for lane-change classification and prediction of surrounding vehicles,” *IEEE Transactions on Intelligent Vehicles*, 2022.
- [6] I. Baek, A. Davies, G. Yan *et al.*, “Real-time detection, tracking, and classification of moving and stationary objects using multiple fisheye images,” in *IEEE Intelligent Vehicles Symposium(IV)*, 2018, pp. 447–452.
- [7] Z.-Q. Zhao, P. Zheng, S.-t. Xu *et al.*, “Object detection with deep learning: A review,” *IEEE Transactions on Neural Networks and Learning Systems*, vol. 30, no. 11, pp. 3212–3232, 2019.
- [8] Q. Song, H. Wang, L. Yang *et al.*, “Double parallel branches fcos for human detection in a crowd,” *Multimedia Tools and Applications*, pp. 1–17, 2022.
- [9] Y. Wang, C. Han, G. Yao *et al.*, “Mapd: An improved multi-attribute pedestrian detection in a crowd,” *Neurocomputing*, vol. 432, pp. 101–110, 2021.
- [10] Z. Chen and X. Huang, “Pedestrian detection for autonomous vehicle using multi-spectral cameras,” *IEEE Transactions on Intelligent Vehicles*, vol. 4, no. 2, pp. 211–219, 2019.
- [11] Z. Wu, W. Zhang, J. Wang *et al.*, “Disentangling and vectorization: A 3d visual perception approach for autonomous driving based on surround-view fisheye cameras,” in *IEEE/RJS International Conference on Intelligent Robots and Systems(IROS)*, 2021, pp. 5576–5582.
- [12] L. Li, M. Yang, H. Li *et al.*, “Robust localization for intelligent vehicles based on compressed road scene map in urban environments,” *IEEE Transactions on Intelligent Vehicles*, 2022.
- [13] P. Dollár, C. Wojek, B. Schiele *et al.*, “Pedestrian detection: An evaluation of the state of the art,” *IEEE Transactions on Pattern Analysis and Machine Intelligence(TPAMI)*, vol. 34, no. 4, pp. 743–761, 2011.
- [14] A. Geiger, P. Lenz, and R. Urtasun, “Are we ready for autonomous driving? the kitti vision benchmark suite,” in *Conference on Computer Vision and Pattern Recognition(CVPR)*, 2012, pp. 3354–3361.

- [15] S. Zhang, R. Benenson, and B. Schiele, "Citypersons: A diverse dataset for pedestrian detection," in *Conference on Computer Vision and Pattern Recognition(CVPR)*, 2017, pp. 3213–3221.
- [16] S. Zhang, Y. Xie, J. Wan *et al.*, "Widerperson: A diverse dataset for dense pedestrian detection in the wild," *IEEE Transactions on Multimedia*, vol. 22, no. 2, pp. 380–393, 2019.
- [17] S. Yogamani, C. Hughes, J. Horgan *et al.*, "Woodscape: A multi-task, multi-camera fisheye dataset for autonomous driving," in *IEEE International Conference on Computer Vision(ICCV)*, 2019, pp. 9308–9318.
- [18] A. K. Cheria and E. Poovammal, "Image augmentation using hybrid ransac algorithm," *Webology*, vol. 18, no. Special Issue on Information Retrieval and Web Search, pp. 237–254, 2021.
- [19] T. Liesting, F. Frasinca, and M. M. Trușcă, "Data augmentation in a hybrid approach for aspect-based sentiment analysis," in *ACM Symposium on Applied Computing*, 2021, pp. 828–835.
- [20] G. Ghiasi, Y. Cui, A. Srinivas *et al.*, "Simple copy-paste is a strong data augmentation method for instance segmentation," in *Conference on Computer Vision and Pattern Recognition(CVPR)*, 2021, pp. 2918–2928.
- [21] T.-Y. Lin, M. Maire, S. Belongie *et al.*, "Microsoft coco: Common objects in context," in *European Conference on Computer Vision(ECCV)*, 2014, pp. 740–755.
- [22] P. Dollár, C. Wojek, B. Schiele *et al.*, "Pedestrian detection: A benchmark," in *Conference on Computer Vision and Pattern Recognition(CVPR)*, 2009, pp. 304–311.
- [23] S. Hwang, J. Park, N. Kim *et al.*, "Multispectral pedestrian detection: Benchmark dataset and baseline," in *Conference on Computer Vision and Pattern Recognition(CVPR)*, 2015, pp. 1037–1045.
- [24] W. Ouyang and X. Wang, "A discriminative deep model for pedestrian detection with occlusion handling," in *Conference on Computer Vision and Pattern Recognition(CVPR)*, 2012, pp. 3258–3265.
- [25] B. Wu and R. Nevatia, "Detection of multiple, partially occluded humans in a single image by bayesian combination of edgelet part detectors," in *IEEE International Conference on Computer Vision(ICCV)*, vol. 1, 2005, pp. 90–97.
- [26] T.-Y. Lin, P. Goyal, R. Girshick *et al.*, "Focal loss for dense object detection," in *IEEE International Conference on Computer Vision(ICCV)*, 2017, pp. 2980–2988.
- [27] L. Ma, Y. Chen, and J. Zhang, "Vehicle and pedestrian detection based on improved yolov4-tiny model," in *Journal of Physics: Conference Series*, vol. 1920, no. 1, 2021, p. 012034.
- [28] J. Redmon, S. Divvala, R. Girshick *et al.*, "You only look once: Unified, real-time object detection," in *Conference on Computer Vision and Pattern Recognition(CVPR)*, 2016, pp. 779–788.
- [29] Y. Wu, Y. Chen, L. Yuan *et al.*, "Rethinking classification and localization for object detection," in *Conference on Computer Vision and Pattern Recognition(CVPR)*, 2020, pp. 10 186–10 195.
- [30] J. Li, X. Liang, S. Shen *et al.*, "Scale-aware fast r-cnn for pedestrian detection," *IEEE Transactions on Multimedia*, vol. 20, no. 4, pp. 985–996, 2017.
- [31] C.-Y. Fu, W. Liu, A. Ranga *et al.*, "Dssd: Deconvolutional single shot detector," *arXiv preprint arXiv:1701.06659*, 2017.
- [32] W. Liu, D. Anguelov, D. Erhan *et al.*, "Ssd: Single shot multibox detector," in *European Conference on Computer Vision(ECCV)*, 2016, pp. 21–37.
- [33] C. Yan, H. Zhang, X. Li *et al.*, "R-ssd: refined single shot multibox detector for pedestrian detection," *Applied Intelligence*, pp. 1–18, 2022.
- [34] B. X. Zhang S, Wen L, "Single-shot refinement neural network for object detection," in *Conference on Computer Vision and Pattern Recognition(CVPR)*, 2018.
- [35] Q. Chen, Y. Wang, T. Yang *et al.*, "You only look one-level feature," in *Conference on Computer Vision and Pattern Recognition(CVPR)*. IEEE, 2021, pp. 13 039–13 048.
- [36] G. Li, Z. Ji, X. Qu *et al.*, "Cross-domain object detection for autonomous driving: A stepwise domain adaptative yolo approach," *IEEE Transactions on Intelligent Vehicles*, 2022.
- [37] S. Ren, K. He, R. Girshick *et al.*, "Faster r-cnn: Towards real-time object detection with region proposal networks," *Conference on Neural Information Processing Systems(NIPS)*, vol. 28, 2015.
- [38] K. He, G. Gkioxari, P. Dollár *et al.*, "Mask r-cnn," in *IEEE International Conference on Computer Vision(ICCV)*, 2017, pp. 2961–2969.
- [39] Y. He, N. He, R. Zhang *et al.*, "Multi-scale feature balance enhancement network for pedestrian detection," *Multimedia Systems*, pp. 1–11, 2022.
- [40] H. Xia, J. Ma, J. Ou *et al.*, "Pedestrian detection algorithm based on multi-scale feature extraction and attention feature fusion," *Digital Signal Processing*, vol. 121, p. 103311, 2022.
- [41] P. Yang, G. Zhang, L. Wang *et al.*, "A part-aware multi-scale fully convolutional network for pedestrian detection," *IEEE Transactions on Intelligent Transportation Systems(TITS)*, vol. 22, no. 2, pp. 1125–1137, 2020.
- [42] H. Zhang, Z. Hu, and R. Hao, "Joint information fusion and multi-scale network model for pedestrian detection," *The Visual Computer*, vol. 37, no. 8, pp. 2433–2442, 2021.
- [43] X. Wang, T. Xiao, Y. Jiang *et al.*, "Repulsion loss: Detecting pedestrians in a crowd," in *Conference on Computer Vision and Pattern Recognition(CVPR)*, 2018, pp. 7774–7783.
- [44] S. Liu, D. Huang, and Y. Wang, "Adaptive nms: Refining pedestrian detection in a crowd," in *Conference on Computer Vision and Pattern Recognition(CVPR)*, 2019, pp. 6459–6468.
- [45] S. Zhang, J. Yang, and B. Schiele, "Occluded pedestrian detection through guided attention in cnns," in *Computer Vision and Pattern Recognition*, 2018, pp. 6995–7003.
- [46] T. DeVries and G. W. Taylor, "Improved regularization of convolutional neural networks with cutout," *arXiv preprint arXiv:1708.04552*, 2017.
- [47] C. Shorten and T. M. Khoshgoftaar, "A survey on image data augmentation for deep learning," *Journal of Big Data*, vol. 6, no. 1, pp. 1–48, 2019.
- [48] E. Arazo, D. Ortego, P. Albert *et al.*, "Pseudo-labeling and confirmation bias in deep semi-supervised learning," in *International Joint Conference on Neural Networks*, 2020, pp. 1–8.
- [49] S. Yun, D. Han, S. J. Oh *et al.*, "Cutmix: Regularization strategy to train strong classifiers with localizable features," in *IEEE International Conference on Computer Vision(ICCV)*. IEEE, 2019, pp. 6023–6032.
- [50] D. Dwibedi, I. Misra, and M. Hebert, "Cut, paste and learn: Surprisingly easy synthesis for instance detection," in *IEEE International Conference on Computer Vision(ICCV)*, 2017, pp. 1301–1310.
- [51] B. C. Russell, A. Torralba, K. P. Murphy *et al.*, "Labelme: a database and web-based tool for image annotation," *International Journal of Computer Vision*, vol. 77, no. 1, pp. 157–173, 2008.
- [52] W. Liu, Z. Piao, J. Min *et al.*, "Liquid warping gan: A unified framework for human motion imitation, appearance transfer and novel view synthesis," in *IEEE International Conference on Computer Vision(ICCV)*, 2019, pp. 5904–5913.
- [53] K. Duan, S. Bai, L. Xie, H. Qi, Q. Huang, and Q. Tian, "Centernet: Keypoint triplets for object detection," in *IEEE International Conference on Computer Vision(ICCV)*, 2019, pp. 6569–6578.
- [54] F. Yu, D. Wang, E. Shelhamer *et al.*, "Deep layer aggregation," in *Conference on Computer Vision and Pattern Recognition(CVPR)*, 2018, pp. 2403–2412.
- [55] Z. Cai and N. Vasconcelos, "Cascade r-cnn: high quality object detection and instance segmentation," *IEEE transactions on pattern analysis and machine intelligence*, vol. 43, no. 5, pp. 1483–1498, 2019.
- [56] C. Szegedy, S. Ioffe, V. Vanhoucke *et al.*, "Inception-v4, inception-resnet and the impact of residual connections on learning," in *AAAI Conference on Artificial Intelligence(AAAI)*, 2017.